Use of Derivative Probes in Spherical Near-Field Antenna Measurements

Kyriakos Kaslis, *Member, AMTA.*
DTU Space - National Space Institute
Technical University of Denmark
Kgs. Lyngby, Denmark
kykas@space.dtu.dk

Olav Breinbjerg, *Fellow, AMTA.*
ElMaReCo
Copenhagen, Denmark
olavbreinbjerg@outlook.com

***Abstract*—The sampling of the field first-order spatial derivative, in addition to the field itself, enables an increase of the sampling step to twice that of the standard sampling criterion – and thus facilitates a reduction of the measurement time. Here, we investigate so-called derivative probes and their usage for spherical near-field antenna measurements.**

I. Introduction

The principle of sampling a signal derivative in addition to the signal itself was suggested by Shannon in 1949 [1]. An early application of this principle to antenna measurements was reported by Corey and O'Neil for planar near-field antenna measurements in 1985-86 [2]-[3], and recently by the present authors for spherical near-field antenna measurements in 2022-24 [4]-[8]. These works demonstrated that the sampling of the signal as well as the signal derivative enables the sampling step to be increased to twice – and thus the number of sampling points to be reduced to half – that of the standard sampling criterion. Obviously, this reduction of sampling points may facilitate a corresponding reduction of the measurement time.

Our 2023 AMTA paper [6] investigated the feasibility of derivative sampling assuming that the probe signal derivative was known – from either a spectrum of the probe signal or from two nearby probe signal samples using the finite difference ratio. The focus was on the use of the probe signal derivative rather than on the measurement of this derivative.

The objective of the present work is to investigate various aspects of probe antennas for measuring field derivatives. An antenna capable of providing one signal related to the incident field as well as another signal related to the spatial derivative of the incident field may be referred to as a *derivative probe* – as opposed to a *standard probe* providing only the former signal. To the authors' best knowledge, such a derivative probe has not yet been developed and employed for antenna measurements. Indeed, for all experiments reported in the abovementioned works, the derivative was obtained from two nearby probe signal samples using the finite difference ratio. Though this may also be a practical procedure if employed with oscillating scans [6]-[7], it will be more efficient using an actual derivative probe.

With a standard probe, the measurement system does not sample exactly the field but a quantity closely related to the field - with the influence of the probe being known and expressed in terms of the standard probe receiving coefficients. Similarly, derivative probes need not sample exactly the derivative of the field but just a quantity closely related to the derivative – as long as the influence of the derivative probe is known and expressed in terms of the derivative probe receiving coefficients. The essential point is to sample, in each sampling point, two sufficiently independent quantities enabling the solution of the near-field transmission formula.

This paper is organized as follows: Section II presents a numerical investigation, based on experimentally measured data and thus including measurement noise, for a derivative probe of non-zero extent; this probes measures neither the field nor the field derivative in a single point but quantities related to these – with its influence expressed in terms of probe receiving coefficients. Section III recalls the sum and difference pattern property of the mono-pulse antenna known from radar technology since this may form the basis for the design of derivative probes; this Section also presents designs of simple derivative probes based on open-ended rectangular wave guides with proper excitations as well as the spherical wave expansions for these derivative probes. Finally, Section IV presents conclusions.

II. Derivative Probe Measurement

This Section II presents an experimental/numerical investigation for a full-circle measurement of a C-band antenna under test (AUT) using a derivative probe.

A. Reference Signal and Spectrum

The reference is based on an experimental full-circle (360°) E-plane measurement of a Scientific Atlanta 12-3.9 standard gain horn at 5.3 GHz using a dual-port conical-horn probe at a measurement distance of 6.1 m and employing on-the-fly sampling with a sampling step of 0.1° and a time-wise sampling rate of 147 Hz. Fig. 1 (top) shows the reference spectrum W_n and the reference signal w; these constitute a Fourier series pair,

$$w(u) = \sum_{n=-N}^{N} W_n e^{jnu} , \tag{1a}$$

$$W_n = \frac{\Delta u}{2\pi}\sum_{m=1}^{M} w(u_m)e^{-jnu_m}, \quad \begin{cases} u_m = -\pi + (m-1)\Delta u \\ \Delta u = 2\pi / M \\ M \geq 2N+1 \end{cases} . \quad (1b)$$

The AUT minimum sphere gives a truncation number N = 44 and thus a standard sampling step of 4°. With the much smaller sampling step of 0.1°, corresponding to a truncation number N = 1799, it is possible to isolate the higher-order modes representing measurement noise to study the effect of this on the performance of the derivative sampling. Fig. 1 (bottom) shows the signal w^{44} based on the part of the spectrum with N = 44, the signal w^{1799} based on the entire spectrum, and the equivalent error signal (EES) possessing an RMS of -64 dB. Hence, the measurement has a good signal-to-noise ratio, but it could be even better using a lower sampling rate than 147 Hz.

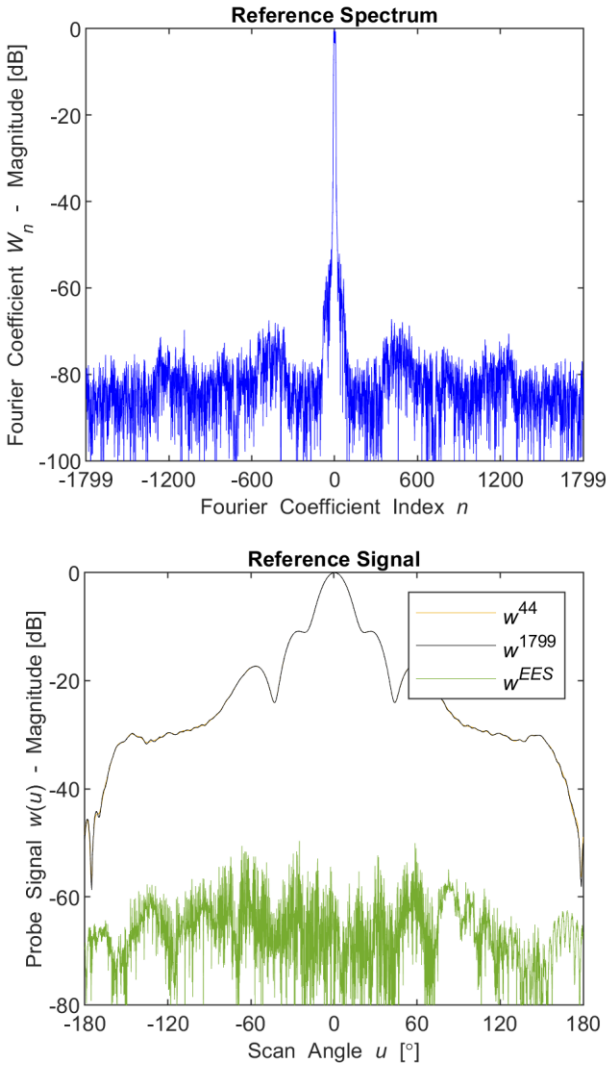

Figure 1. Top: reference spectrum based on measurement with Δu = 0.1° and thus truncation number N = 1799. Bottom: reference signals based on reference spectrum with N = 44 and N = 1799, respectively, as well the equivalent error signal quantifying their difference; RMS(EES) = -64 dB.

B. Derivative Probe Model and Measurement

The employed derivative probe consists of an even number L of point elements positioned along the measurement circle with angular separation ΔL, see Fig. 2; each element gives a signal according to (1a). The derivative probe has 2 ports, a sum port and a difference-port, the signals of which can be expressed as

$$\begin{Bmatrix} w^{sum}(u) \\ w^{dif}(u) \end{Bmatrix} = \sum_{l=L/2+1}^{L} w(u_l) \begin{Bmatrix} + \\ - \end{Bmatrix} \sum_{l=1}^{L/2} w(u_l) \quad (2a)$$

where u_l is the position of the l'th element

$$u_l = u - (L+1-2l)\Delta L/2 . \quad (2b)$$

An example of the derivative probe patterns is shown in Fig. 3.

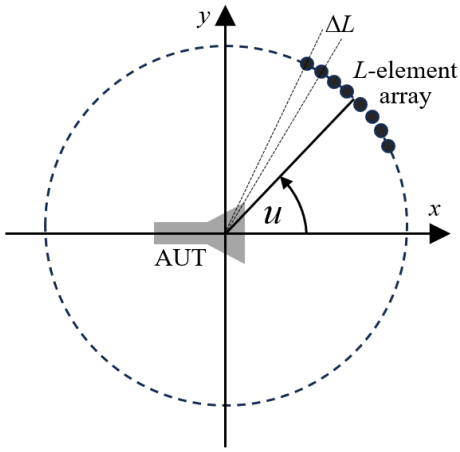

Figure 2. Derivative probe formed as an array of L point elements positioned along the measurement circle with angular separation ΔL.

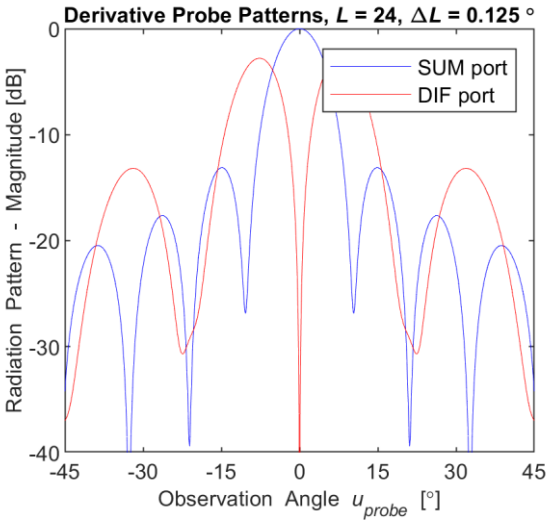

Figure 3. Derivative probe radiation patterns. The probe has L = 24 point elements with angular separation ΔL = 0.125°.

The received signals at the sum and difference ports of the derivative probe can be obtained numerically using (2) with the signal for each element calculated from (1a) with the reference spectrum in Fig. 1. While the standard sampling of only the signal requires a sampling step $\Delta u = 4°$, the use of the derivative probe allows the sampling step to be $\Delta u = 8°$. The obtained sum- and difference-port signals are shown in Fig. 4; in this case, the entire spectrum is used with $N = 1799$ to include the effect of measurement noise. The sum-port signal obviously resembles the reference signal in Fig. 1; but in itself it is under-sampled by a factor of 2. The difference-port signal is of course notably weaker – due to the on-axis null of the radiation pattern seen in Fig. 3 – but largely, it remains well above the -64 dB noise level seen in Fig. 1.

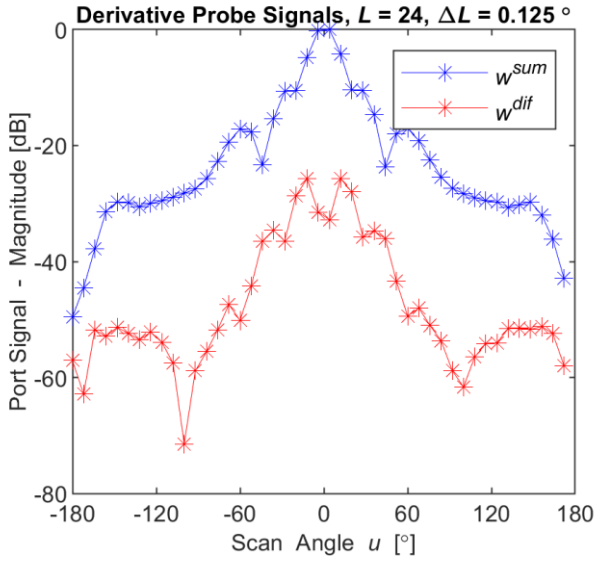

Figure 4. Signals received at the sum and difference ports of the derivative probe of Fig. 2 using the spectrum of Fig. 1 with $N = 1799$ and a sampling step $\Delta u = 8°$.

C. Probe Correction

Inserting the signal Fourier series (1a) into (2a), interchanging the two summations, and evaluating the inner summation, the sum- and difference port signals can be expressed as

$$\begin{Bmatrix} w^{sum}(u) \\ w^{dif}(u) \end{Bmatrix} = \sum_{n=-N}^{N} \begin{Bmatrix} W_n^{sum} \\ W_n^{dif} \end{Bmatrix} e^{jnu} \quad , \tag{3a}$$

with the port spectral coefficients related to the signal spectral coefficients by

$$\begin{Bmatrix} W_n^{sum} \\ W_n^{dif} \end{Bmatrix} = \begin{Bmatrix} R_n^{sum} \\ R_n^{dif} \end{Bmatrix} W_n \, , \tag{3b}$$

where the port spectral receiving coefficients are

$$R_n^{sum} = \frac{\sin(nL\Delta L/2)}{\sin(n\Delta L/2)} \, , \tag{3c}$$

$$R_n^{dif} = 2j\frac{\sin^2(nL\Delta L/4)}{\sin(n\Delta L/2)} \, . \tag{3d}$$

Using eqs. (3a)-(3d), it is obviously possible to establish a system of linear equations from which the signal spectral coefficients W_n can be obtained from the probe sum- and difference-port signals $w^{sum}(u)$ and $w^{dif}(u)$ at half the number of standard sampling points – provided that the system is well conditioned.

There exists, however, a more efficient and stable approach consisting of the following steps: First, use the inverse of (3a) to determine the port spectral coefficients from the sum- and difference-port signals and; thus, in line with (1b), we have

$$\tilde{W}_n^{\begin{Bmatrix} sum \\ dif \end{Bmatrix}} = \frac{\Delta u}{2\pi} \sum_{m=1}^{M_H} w^{\begin{Bmatrix} sum \\ dif \end{Bmatrix}}(u_m) e^{-jnu_m} \tag{4a}$$

with

$$\begin{cases} u_m = -\pi + (m-1)\Delta u \\ \Delta u = 2\pi / M_H \\ M_H \geq N+1 \end{cases} \tag{4b}$$

The tilda sign indicates that the obtained coefficient is different from the correct coefficient due to the use of only (approximately) half the number of standard sampling points, $M_H \geq N+1$ as opposed to $M \geq 2N+1$. However, it can be shown that each obtained coefficient is the aliasing of two correct coefficients,

$$\tilde{W}_n^{\begin{Bmatrix} sum \\ dif \end{Bmatrix}} = \begin{cases} W_n^{\begin{Bmatrix} sum \\ dif \end{Bmatrix}} + (-1)^{M_H} W_{n+M_H}^{\begin{Bmatrix} sum \\ dif \end{Bmatrix}}, & n \leq -1 \\ W_0^{\begin{Bmatrix} sum \\ dif \end{Bmatrix}}, & n = 0 \\ W_n^{\begin{Bmatrix} sum \\ dif \end{Bmatrix}} + (-1)^{M_H} W_{n-M_H}^{\begin{Bmatrix} sum \\ dif \end{Bmatrix}}, & n \geq 1 \end{cases} \tag{5}$$

The sum and difference parts of (5) each constitutes two equations with two unknowns, which can readily be solved to determine the correct port spectral coefficients – and from these follows by (3b) the signal spectral coefficients. Hence, the second step can be expressed as

$$W_n = \begin{cases} \dfrac{\tilde{W}_n^{sum} R_{n+M_H}^{dif} - \tilde{W}_n^{diff} R_{n+M_H}^{sum}}{R_n^{sum} R_{n+M_H}^{dif} - R_n^{dif} R_{n+M_H}^{sum}}, & n \leq -1 \\ \tilde{W}_0^{sum}/L, & n = 0 \\ \dfrac{\tilde{W}_n^{sum} R_{n-M_H}^{dif} - \tilde{W}_n^{diff} R_{n-M_H}^{sum}}{R_n^{sum} R_{n-M_H}^{dif} - R_n^{dif} R_{n-M_H}^{sum}}, & n \geq 1 \end{cases} \, . \tag{6}$$

In summary, from the measured derivative probe sum- and difference-port signals $w^{sum}(u)$ and $w^{dif}(u)$ at (approximately) half the number of standard sampling points, $M_H \geq N+1$, the use of first (4) and second (6) will determine the signal spectral coefficients W_n. This approach is employed below.

D. Retrieved Signal

In the ideal noise-free case with no higher-order spectral components above those due to the AUT, in which case the sampling criterion $M_H \geq N+1$ would be satisfied, the probe correction outlined in Subsection II.C gives the exact signal coefficients W_n. Hence, for derivative probe signals (3) based on the signal w^{44} in Fig. 1, with sampling step $\Delta u = 8°$, the probe correction, with (4) and (6), exactly recovers the signal coefficient W_n, $n \leq 44$.

In the practical noisy case with higher-order spectral components above those due to the AUT, the probe correction will of course be influenced. We use now the probe signals in Fig. 4, based on reference spectrum for N=1799, with sampling step $\Delta u = 8°$, thus the number of samples $M_H = 45$. Upon retrieval of the spectrum, up to the truncation number 44, the spatial signal is calculated for every 0.1°; Fig. 5 shows a comparison of this retrieved signal with the reference signal w^{44} of Fig. 1. It is seen that the retrieved signal agrees well with the reference signal, the RMS of the EES is only -66 dB.

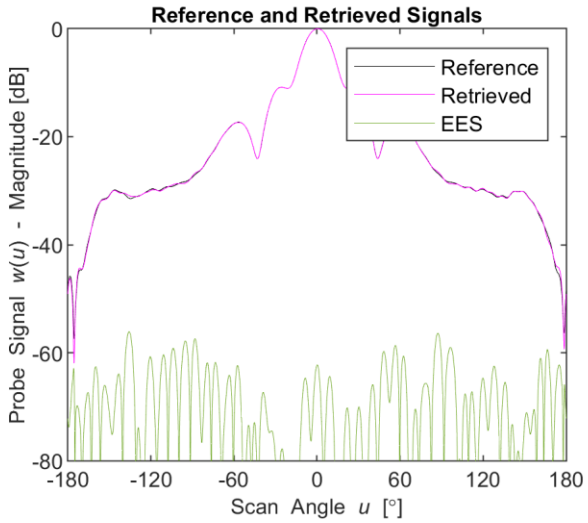

Figure 5. Comparison of reference signal w^{44} with retrieved signal based on derivative probe measurement shown in Fig. 4 as well the equivalent error signal quantifying their difference; RMS(EES) = -66 dB.

Similar comparisons have been made for derivative probes with different number of elements, and Table I lists the obtained EES. With increasing number of elements, the probe sum and difference signals will differ increasingly from the ideal point signal and signal derivative; yet the EES actually decreases. This must be due to the fact that more elements also serve to reduce the effect of measurement noise through the averaging of this over the number of elements. These results demonstrate that the derivative probe does not need to provide precisely the signal and the signal derivative in a single point – but just quantities related to these as long as the influence of the probe can be compensated for with probe correction.

TABLE I. EQUIVALENT ERROR SIGNAL BETWEEN REFERENCE AND RETRIEVED SIGNALS FOR DIFFERENT NUMBERS OF DERIVATIVE PROBE ELEMENTS

No. of elements L	RMS(EES) [dB]
2	-48
4	-56
8	-62
12	-63
16	-64
20	-65
24	-66

E. Summary

The derivative probe does not measure exactly the field/signal and its spatial first-order derivative; but it measures quantities sufficiently close to these and thus provides two independent samples at each sampling point; hence the number of sample points can be reduced to half of the standard number. The experimental/numerical investigation in this Section II has demonstrated that upon probe correction, a measurement with a derivative probe can recover the reference signal to a very high accuracy even in the presence of realistic measurement noise.

III. DERIVATIVE PROBE – SIMPLE DESIGNS

This Section III discusses the design of derivative probes based on rectangular waveguide technology.

A. Background - Monopulse Antennas

A derivative probe should have one port providing a signal related to the incident field itself as well as a second port providing a signal related to a spatial derivative of the incident field. As demonstrated in Section II, see Fig. 3, the port for the field itself could have a sum radiation pattern while the port for the field derivative could have a difference pattern; indeed, the two ports can be referred to as the sum port and the difference port, respectively. Hence, the design of derivative probes could well exploit the heritage of so-called mono-pulse antennas which are widely used for radar tracking, electronic support measure, and direction estimation in general [10]-[11].

The mono-pulse technology developed from the 1940s in both the East [12] and the West [13] and of course first for military purposes; the proper processing of the sum- and difference-port signals facilitates a very accurate direction estimation. Later, its usage expanded to satellite tracking, not least with low Earth orbit constellations where passage times are short, to mobile satellite communication, and more recently also to automotive radars, drone technology, internet-of-things systems, mobile communication, and WLAN for tracking of individual devices and users. Numerous antenna types have been employed for mono-pulse systems in the different application areas – as overviewed in e.g. [14]-[16].

For antenna measurements, it would be a natural extension from standard probes to employ single-horn antennas for derivative probes – aiming at maintaining the reasonable bandwidth, the high radiation efficiency, the high polarisation purity, the low scattering cross section, and possibly pattern

characteristics facilitating an efficient and stable solution of the near-field transmission formula.

B. *Derivative Probes using Rectangular Waveguide Modes*

Reference [7] discusses how the rectangular waveguide TE_{10}, TE_{20}, and HEM_{11} modes may be employed for the sum port and two difference ports - one for derivative in direction perpendicular to polarization, the other for derivative in direction parallel to polarization. The rectangular single-horn mono-pulse antennas reported by e.g. [17] -[20] were indeed based on these, and in some cases also higher-order, waveguide modes.

Fig. 6 shows a conceptual arrangement of 4 coaxial probe feeds into the square waveguide and the combinations of the feed signals to excite the *y*-polarized TE_{10}, TE_{20}, and HEM_{11} modes, as well as the corresponding electric fields over the cross section of the waveguide.

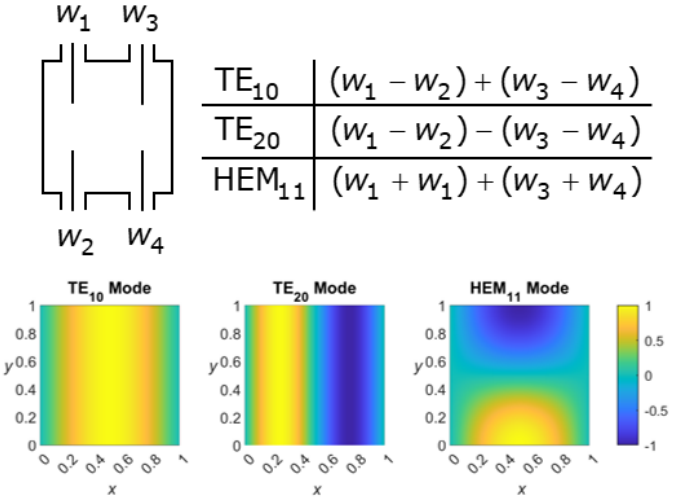

Figure 6. Top: square waveguide cross section ($0 \le x \le 1$, $0 \le y \le 1$) with 4 coaxial probe feeds and combinations of the probe feed signals for the TE_{10}, TE_{20}, and HEM_{11} waveguide modes. Bottom: electric field *y*-component.

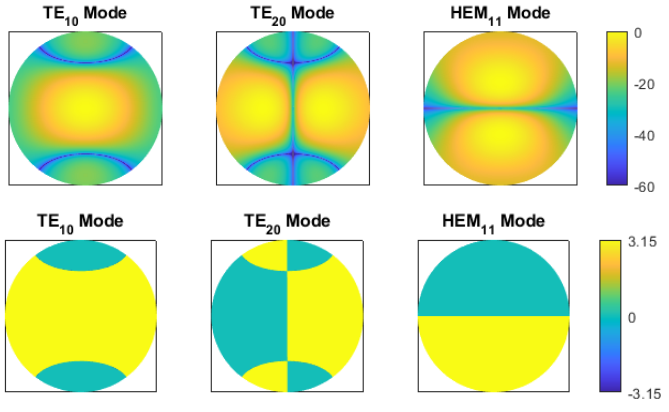

Figure 7. Radiated co-polar far-fields (polar plots with $0 \le \theta \le 90°$ in radial direction and $0 \le \phi < 360°$ in azimuthal direction) for aperture size $a = 1.25\lambda$. Top: Magnitude [dB]. Bottom: Phase [rad].

Fig. 7 shows the radiated far-fields of the open-ended waveguide based on both equivalent electric and magnetic currents and assuming aperture fields equal to the waveguide mode fields. For TE_{10} waveguide mode, the far-field is of course the typical sum-pattern of a standard probe. For the TE_{20} waveguide mode, the far-field is a difference pattern for the *x*-derivative of the *y*-component of the field; and for the HEM_{11} waveguide mode, the far-field is a difference pattern for the *y*-derivative of the *y*-component of the field.

C. *Spherical Wave Expansion and Solution of the Spherical Near-Field Transmission Formula*

In the following, we employ the spherical wave expansion (7), where $\boldsymbol{E}$ is the electric field, $\boldsymbol{r}$ the position vector, k the wave number, η the intrinsic admittance of ambient medium, $Q^{(3)}_{smn}$ the so-called Q-coefficients, $\boldsymbol{F}^{(3)}_{smn}$ the out-going spherical vector wave functions (modes), and N is the truncation number [9];

$$\boldsymbol{E}(\boldsymbol{r}) = \frac{k}{\sqrt{\eta}} \sum_{s=1}^{2} \sum_{n=1}^{N} \sum_{m=-n}^{n} Q^{(3)}_{smn} \boldsymbol{F}^{(3)}_{smn}(\boldsymbol{r}) \,. \tag{7}$$

Standard probes are ideally so-called first-order probes with spectra containing only azimuthal modes of order $m = \pm 1$ since such probe facilitate the standard efficient and stable solution of the transmission formula [9]; this is often referred to as first-order probe correction. However, not all standard probes are first order and in such cases higher-order probe correction becomes necessary [21].

Based on the full-sphere (enabled by the use of both electric and magnetic equivalent currents) far-fields in Section III.B, the corresponding spherical wave expansions (SWEs) (7) have been calculated; see Fig. 8. As expected, the SWE for the radiated field of the TE_{10} waveguide mode is dominated by the $m = \pm 1$ spherical modes while the SWEs for the TE_{20} and HEM_{11} waveguide modes are dominated by the $m = 0$ and $m = \pm 2$ spherical modes.

IV. Conclusions

Based on experimental measurement data including measurement noise, it has been demonstrated in Section II that the use of a derivative probe of non-zero extent, having both a sum and a difference port/pattern, enables the sampling step to be increased to twice that of the standard sampling criterion. The derivative probe samples quantities closely related to the field and its spatial derivative, and the influence of the derivative probe receiving coefficients is compensated for with probe correction.

Simple derivative probe designs based on square waveguides with proper TE_{10}, TE_{20}, and HEM_{11} excitations have been presented in Section III along with their radiated far-field and spherical wave expansions. While standard probes are dominated by $m = \pm 1$ spherical modes, the derivative probes are dominated by the $m = 0$ and $m = \pm 2$ spherical modes.

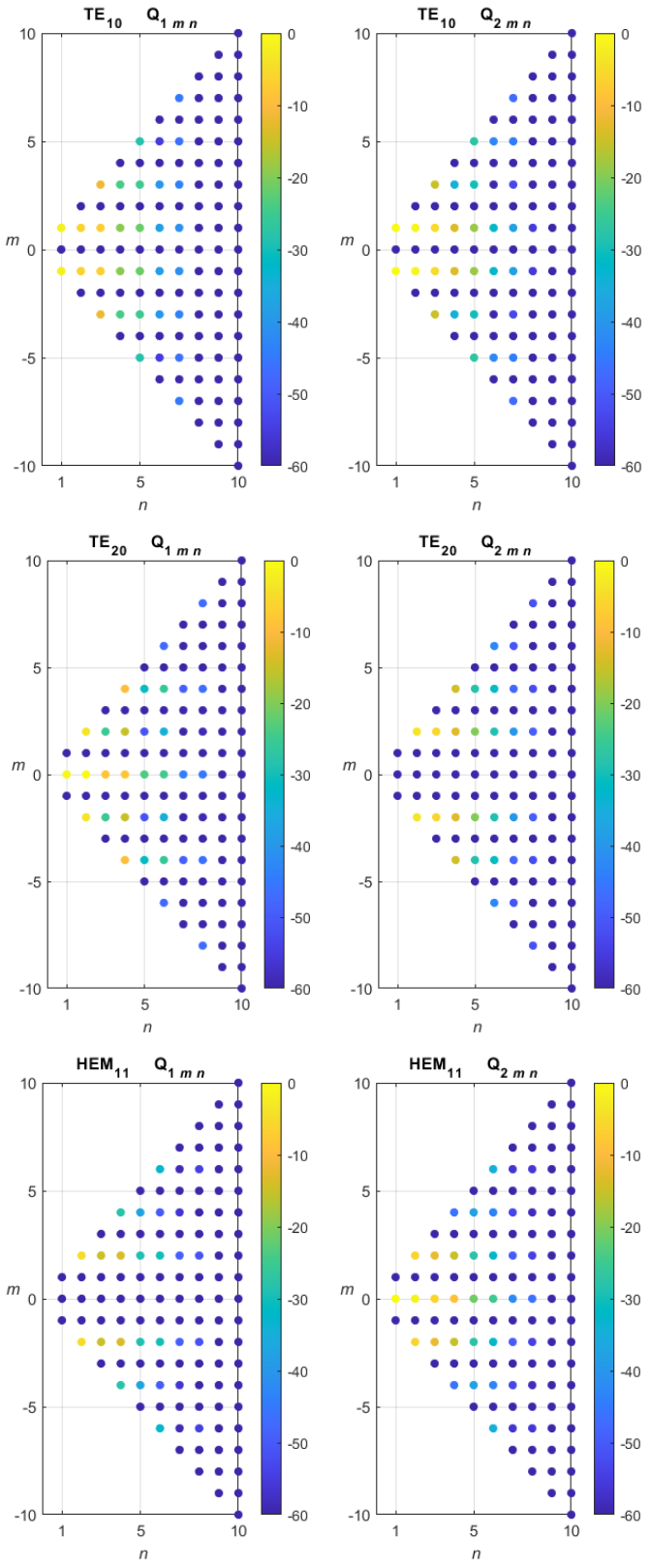

Fig. 8. Spherical wave expansion Q-coefficients for the far-fields in Fig. 7 of the TE_{10}, TE_{20}, and HEM_{11} rectangular waveguide modes in Fig. 6.

REFERENCES

[1] C.E. Shannon, "Communication in the Presence of Noise", *Proceedings of the IRE*, pp. 10-21, January 1949.

[2] L.E. Corey and D.R. O'Neil, "Alternative Sampling Techniques for More Efficient Planar Near-Field Measurements", *AMTA Annual Meeting and Symposium*, pp. 7-1 – 7-10, 1985.

[3] L.E. Corey and D.R. O'Neil, "Differential Sampling of Planar Near-Fields", *IEEE Antennas and Propagation Society International Symposium*, pp. 191-194, Philadelphia, PA, USA, June 1986.

[4] K. Kaslis, O. Breinbjerg, " Potentially Fast Spherical Near-Field Measurements for General Antennas based on Signal Derivatives, 16th *European Conference on Antennas and Propagation*, Madrid, March 2022.

[5] K. Kaslis, S. Arslanagic, and O. Breinbjerg, "Experimental Test of Employing Probe Signal Derivatives in Near-Field Antenna Measurements", *IEEE International Symposium of Antennas and Propagation*, Portland, Oregon, 2023.

[6] K. Kaslis and O. Breinbjerg "On the Use of Probe Signal Derivatives in Spherical Near-Field Antenna Measurements", *45th AMTA Annual Meeting and Symposium*, Seattle, Washington, October 2023.

[7] O. Breinbjerg, "Derivative Sampling of Periodic and Non-Periodic Band-Limited Signals – Fourier Spectrum and Interpolation Formula", *IEEE Trans. Antennas Propagat.*, accepted for publication, July 2024.

[8] K. Kaslis, S. Arslanagic, and O. Breinbjerg, "Experimental Proof-of-Concept for Use of Probe Signal Derivatives in Spherical Near-Field Antenna Measurements", *IEEE Antennas and Wireless Propagation Letters*, in submission, May 2024.

[9] J.E. Hansen, "Spherical Near-Field Antenna Measurements", Peter Perigrinus, 1988.

[10] S.M. Sherman, "Monopulse Principles and Techniques", Artech House, Dedham, Massachusets, 1984.

[11] D.K. Barton and S.M. Sherman, "Monopulse Principles and Techniques", 2nd edition, Artech House, Boston and London, Norwood, Massachusetts, 2011.

[12] A.I. Leonov, "History of Monopulse Radar in the USSR", *IEEE Aerospace Electronic Systems Society Magazine*, pp. 7-13, May 1998.

[13] D.K. Barton, "History of Monopulse Radar in the US", *IEEE Aerospace Electronic Systems Society Magazine,* Historical Publication insert, March 2010.

[14] A. Gil-Martinez et al., "Monopulse Leaky Wave Antennas for RSSI-Based Direction Finding in Wireless Local Area Networks", *IEEE Trans. Antennas Propagat.*, vol. 71, no. 11, pp. 8602-8615, Nov. 2023.

[15] X. Jiang et al., "A Compact Ka-Band Low-Sidelobe Monopulse Antenna Array Based on Mixed Gap Waveguide and Hollow Waveguide Multilayer Feeding Network", *IEEE Trans. Antennas Propagat.*, vol. 71, no. 11, pp. 8714-8725, November 2023.

[16] Z. Wang et al., "A Wideband High-Gain Planar Monopulse Array Antenna for Ka-Band Radar Applications", *IEEE Trans. Antennas Propagat.*, vol. 71, no. 11, pp. 8739-8752, November 2023.

[17] C.C. Ling and G.M. Rebeiz, "94 GHz Integrated Horn Monopulse Antennas", *IEEE Trans. on Antennas Propagat.*, vol. 40, no 40, pp. 981-984, August 1992.

[18] R. Shen, X. Ye, and J. Miao, "Design of a Multimode Feed Horn Applied in a Tracking Antenna", *IEEE Trans. Antennas Propagat.*, vol. 65, no. 6, pp. 2779-2788, June 2017.

[19] H. Wang, "Multimode Horn for a Monopulse Subsystem", *IEEE International Symposium on Antennas and Propagation*, Atlanta, Georgia, 2019.

[20] Z. Chen et al., "An E-Band Beam Sharpening Antenna Based on Monopulse Comparator", *IEEE Access*, vol. 9, pp. 73262-73270, 2021.

[21] T. Laitinen et al., "Theory and Practice of the FFT/Matrix Inversion Technique for Probe-Corrected Spherical Near-Field Antenna Measurements With High-Order Probes", *IEEE Trans. Antennas Propagat.*, vol. 58, no. 8, pp. 2623-2631, August 2010.